# Dalton Transactions

Accepted Manuscript






ROYAL SOCIETY OF CHEMISTRY

www.rsc.org/dalton

# Metal(II) Complexes Based on Quinoline-2,3-Dicarboxylate as Electrocatalysts for Degradation of Methyl Orange

**Yun Gong, * Miao Miao Zhang, Jian Bo Qin, Jian Li, Jiang Ping Meng and Jian Hua Lin***

Based on quinoline-2,3-dicarboxylic acid ($H_2L$), two metal(II) complexes with 1D chain-like structures, exhibit electrocatalytic activities for degradation of methyl orange (MO), which is probably associated with their electrocatalytic activities for the $H_2$ evolution reaction from water.

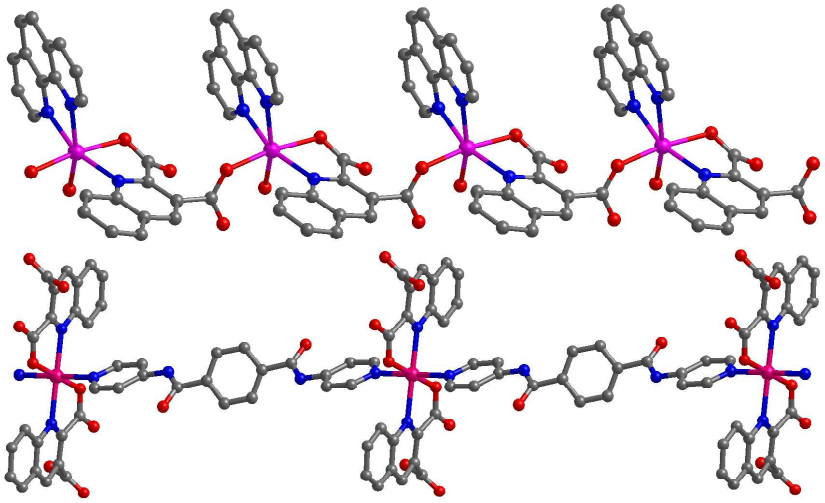

# Metal(II) complexes based on quinoline-2,3-dicarboxylate as electrocatalysts for degradation of methyl orange

**Yun Gong, [*a] Miao Miao Zhang, [a] Jian Bo Qin, [a] Jian Li, [a] Jiang Ping Meng [a] and Jian Hua Lin [*a,b]**

[a]*Department of Applied Chemistry, College of Chemistry and Chemical Engineering, Chongqing University, Chongqing 400030, P. R. China Tel: +86-023-65106150 E-mail: gongyun7211@cqu.edu.cn*

[b]*President, Zhejiang University, Hangzhou 310058, P. R. China Tel: +86-0571-88981583 E-mail: jhlin@zju.edu.cn; jhlin@cqu.edu.cn; jhlin@pku.edu.cn*



Based on quinoline-2,3-dicarboxylic acid ($H_2L$), two metal(II) complexes formulated as $MnL(phen)(H_2O)\cdot H_2O$ (phen=1,10-phenanthroline) (**1**) and $Co(HL)_2(PPA)\cdot 4H_2O$ (PPA= $N^1$,$N^4$-di(pyridin-4-yl)terephthalamide) (**2**) were synthesized and structurally characterized by single-crystal X-ray diffractions. Complexes **1** and **2** both exhibit one-dimensional (1D) chain-like structure, in which stable five-membered rings are observed. Different chains are linked by strong π-π stacking interactions into three- dimensional (3D) supramolecular architecture. The two complexes both can increase the degradation rate of methyl orange (MO), which is expected to be associated with their electrocatalytic activities for the $H_2$ evolution reaction from water.

## Introduction

Industrial effluents containing toxic compounds cause serious environmental problems owing to the lack of a general method of treatment. Besides the traditional chemical, physical and biological methods, the purification of dyeing wastewater by electrochemical techniques has been proven to be a very effective method, where it has the simple equipment, easy operation, lower temperature requirements and no sludge formation.[1–3] Usually, the mechanism of the electrodegradation of 4-dimethylamino-azobenzene-4'-sulfonic acid sodium salt (methyl orange, MO) is based on an electrocatalytic oxidation by hydroxyl radical that is generated on the anode.[4] Up to now, some studies have been carried out to develop high performance anodes in respect of high catalytic activity, long life, including Pt, carbon felt, metal oxide such as $PbO_2$, et al.[4–8]

Coordination polymers are infinite network structures in essence and built from metal ions and bridging organic ligands, which have aroused great interest and developed rapidly in recent years, owing to their unique framework structural topologies and a wide range of potential applications in the fields such as sorption, electrical conductivity, smart optoelectronics, magnetism and catalysis, et al. [9-10] Recently, our study has been mainly focused on the synthesis and characterization of novel metal complexes, which show rich structural features and electrocatalytic properties.[11] However, until now metal complexes are rarely explored in the field of electrocatalyst for the electrodegradation of pollutants such as MO.

Based on the situation, herein, we synthesized a rigid ligand, quinoline-2,3-dicarboxylic acid (**$H_2L$**) (**Scheme 1**).[12] It is expected that the ligand is stable under the electrodegradation condition. Based on **$H_2L$**, two metal(II) complexes formulated as $MnL(phen)(H_2O)\cdot H_2O$ (phen=1,10-phenanthroline) (**1**) and $Co(HL)_2(PPA)\cdot 4H_2O$ (PPA= $N^1$,$N^4$-di(pyridin-4-yl) terephthalamide) (**2**) are obtained via hydrothermal technique in moderate yields. The thermal stabilities, UV-vis absorption and catalytic properties of the complexes on the electrodegradation of MO have been investigated.

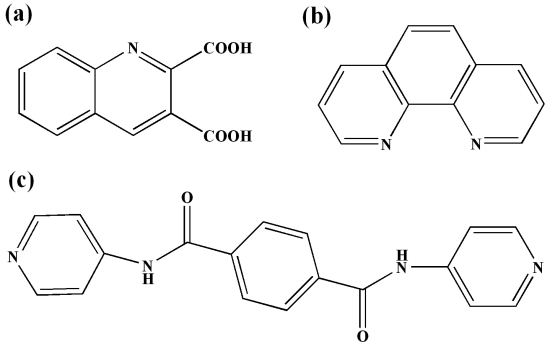


**Scheme 1** The structure of **$H_2L$** (**a**), phen (**b**) and PPA (**c**).

## Experimental

### General Considerations

All chemicals purchased were of reagent grade and used without further purification. The melting point was determined using an uncorrected X-4 melting point apparatus of Beijing Kaifu Company. C, H, N elemental analyses were performed on an Elementar Vario MICRO E III analyzer. IR spectra were recorded as KBr pellets on PerkinElmer spectrometer. The powder XRD (PXRD) data were collected on a RIGAKU DMAX2500PC diffractometer using Cu Kα radiation. TGA was performed on a NETZSCH STA 449C thermogravimetric analyzer in flowing Ar with a heating rate of $10°C\cdot min^{-1}$. UV-Vis spectra were measured on a HITACHI U-4100 UV-vis spectro-photometer. The gas sorption isotherms were measured using a Quadrasorb ZSI-MP-21 volumetric gas adsorption instrument.

### Electrochemical measurements:

The electrochemical measurements were done in a three-electrode test cell. A saturated calomel electrode (SCE) and a platinum foil were used as the reference and counter electrode, respectively. The working electrode was prepared as follows: Ethanol dispersion of 4 mg sample (1 mL) and 0.05 mL of nafion solution were deposited on a glassy carbon electrode (**GCE**) and the solvent is dried by an IR lamp. The electroactive

area of the **GCE** is 0.2 $cm^2$. All the measurements were recorded in 50 mL of $N_2$ degassed solution at 25℃ using a Shiruisi RST5200 electrochemical workstation.

### Synthesis

**Synthesis of $H_2L$:** $H_2L$ was prepared according to the literature method.[12] Melting point: 233℃. IR ($cm^{-1}$): 2817(m), 2494(m), 1865(w), 1728(s), 1701(s), 1619(s), 1571(s), 1500(m), 1459(s), 1403(w), 1383(m), 1345(w), 1282(s), 1204(s), 1150(s), 1139(s), 1052(s), 975(w), 923(s), 866(w), 838(s), 808(s), 774(s), 759(s), 736(s), 655(m).

**Synthesis of MnL(phen)($H_2O$)·$H_2O$ (1)**: A mixture of $MnSO_4·H_2O$ (0.05 mmol, 0.008 g), **$H_2$L** (0.05 mmol, 0.011 g), phen (0.05 mmol, 0.010 g), water (8 ml) and $NH_3.H_2O$ (0.4 ml) was heated at 120 □ in Teflon-lined autoclaves for 3 days, followed by slow cooling to room temperature. The resulting yellow block crystals were filtered off (yield: ca. 62% based on Mn). Elemental Anal. Found: C, 56.84; H, 3.50; N, 8.68%. Calcd. for $C_{23}H_{17}MnN_3O_6$: C, 56.80; H, 3.52; N, 8.64 %. IR (KBr, $cm^{-1}$): 3527(m), 3077(m), 1656(s), 1557(s), 1518(m), 1494(w), 1457(m), 1427(s), 1393(s), 1349(s), 1300(m), 1210(w), 1157(w), 1138(w), 1055(m), 923(w), 847(s), 779(m), 756(m), 728(s), 640(m), 610(m).

**Synthesis of Co(HL)$_2$(PPA)·4$H_2O$ (2)**: The synthesis of complex **2** was carried out as described above for complex **1** except that $CoSO_4·7H_2O$ (0.05 mmol, 0.014 g) and **PPA** (0.05 mmol, 0.016 g) were used instead of $MnSO_4·H_2O$ and phen, respectively. The yield of the red prismatic crystals is ca. 30 % based on Co. Elemental Anal. Found: C, 54.50; H, 3.91; N, 9.50%. Calcd. for $C_{40}H_{34}CoN_6O_{14}$: C, 54.49; H, 3.89; N, 9.53%. IR (KBr, $cm^{-1}$): 3572(s), 3418(s), 2359(m), 1726(m), 1673(m), 1638(s), 1595(s), 1530(s), 1510(s), 1461(m), 1425(m), 1371(s), 1335(s), 1315(s), 1240(m), 1213(m), 1126(w), 1018(m), 831(m), 775(m), 611(m), 536(w).

### X-ray crystallography

Single-crystal X-ray data for complexes **1** and **2** were collected on an Oxford XCalibur Eos diffractometer using graphite monochromated Mo Ka ($\lambda$ = 0.71073 Å) radiation at room temperature. Empirical absorption correction was applied. The structures were solved by direct methods and refined by the full-matrix least-squares methods on $F^2$ using the SHELXTL-97 software.[13] All non-hydrogen atoms were refined anisotropically. The hydrogen atoms attached to coordinated and uncoordinated water molecules were located in the Fourier difference maps. And all of the other hydrogen atoms were placed in the calculated positions. The crystal data and structure refinements for complexes **1** and **2** are summarized in **Table 1**. Selected bond lengths and angles for complexes **1** and **2** are listed in **Table 2**. The CCDC reference numbers are the following: 975535 for complex **1** and 975536 for complex **2**.

**Table 1** Crystal data and structure refinements for complexes **1** and **2**.

| Complex | **1** | **2** |
|---|---|---|
| Empirical formula | $C_{23}H_{17}MnN_3O_6$ | $C_{40}H_{34}CoN_6O_{14}$ |
| *M* | 486.34 | 881.66 |
| Crystal system | triclinic | triclinic |
| Space group | *Pī* | *Pī* |
| *a* /Å | 7.6099(3) | 8.6479(4) |
| *b* /Å | 10.4281(5) | 9.4452(4) |
| *c* /Å | 13.6427(7) | 12.1753(6) |
| α /º | 84.281(4) | 96.438(4) |
| β /º | 89.806(4) | 96.446(4) |
| γ /º | 70.891(4) | 104.773(4) |
| *V* /Å$^3$ | 1017.40(8) | 945.23(8) |
| Z | 2 | 1 |
| $D_{calcd}$/*g* $cm^{-3}$ | 1.588 | 1.549 |
| $\mu$/$mm^{-1}$ | 0.698 | 0.536 |
| No. of unique reflcns | 3449 | 3021 |
| reflcns used [$I > 2\acute{o}(I)$] | 2604 | 2522 |
| F(0 0 0) | 498 | 455 |
| Goodness-of-fit on $F^2$ | 1.025 | 1.042 |
| Final *R* indices [$I>2\sigma(I)$] | $R_1$= 0.0554, $wR_2$= 0.1614 | $R_1$= 0.0305, $wR_2$= 0.0784 |

$R_1=\Sigma||F_0|-|F_c||/\Sigma|F_0|$; $wR_2=\Sigma[w(F_0^2-F_C^2)^2]/\Sigma[w(F_0^2)^2]^{1/2}$

**Table 2** Selected bond lengths (Å) and angles (º) for complexes **1** and **2**.

| | | | |
|---|---|---|---|
| ***Complex 1*** | | | |
| Mn(1)-O(3) | 2.149(3) | Mn(1)-O(5) | 2.171(4) |
| Mn(1)-O(1)#1 | 2.125(3) | Mn(1)-N(2) | 2.257(4) |
| Mn(1)-N(1) | 2.293(3) | Mn(1)-N(3) | 2.327(3) |
| O(3)-Mn(1)-O(5) | 87.24(14) | O(1)#1-Mn(1)-O(3) | 171.90(11) |
| N(2)-Mn(1)-N(3) | 162.74(12) | N(2)-Mn(1)-N(1) | 72.98(13) |
| O(3)-Mn(1)-N(3) | 73.28(12) | O(5)-Mn(1)-N(1) | 163.48(17) |
| ***Complex 2*** | | | |
| Co(1)-O(4) | 2.0208(16) | Co(1)-O(4)#2 | 2.0208(16) |
| Co(1)-N(1) | 2.2274(18) | Co(1)-N(2) | 2.1594(18) |
| O(4)#2-Co(1)-O(4) | 180.0 | N(2)-Co(1)-N(2)#2 | 180.0 |
| N(2)-Co(1)-N(1) | 87.91(7) | N(2)-Co(1)-N(1)#2 | 92.09(7) |
| O(4)-Co(1)-N(1) | 78.21(6) | O(4)-Co(1)-N(1)#2 | 101.79(6) |

Symmetry transformations used to generate equivalent atoms:
#1 x+1, y, z #2 -x+1,-y+2,-z+1

## Results and discussion

**Crystal Structure of MnL(phen)($H_2O$)·$H_2O$ (1)** Single-crystal X-ray diffraction analysis reveals that complex **1** crystallizes in the *triclinic* space group *Pī* (**Table 1**). In complex **1**, the asymmetric unit contains one Mn(II), one $\mathbf{L}^{2-}$, one phen, one coordinated water and one uncoordinated water molecule. The crystallographically independent Mn(1) exhibits a slightly distorted octahedral coordination geometry, defined by two chelating nitrogen atoms from one phen, one pyridine nitrogen atom and two carboxylate oxygen atoms from two $\mathbf{L}^{2-}$ and one oxygen atom from water molecule [Mn-O 2.125(3)-2.171(4) Å, Mn-N 2.257(4)-2.327(3) Å] (**Fig.1a** and **Table 2**). In complex **1**, the crystallographically independent $\mathbf{L}^{2-}$ ligand acts as a $u_2$-bridge linking two Mn(II) centers via two monodentate bridging carboxylate groups into one-dimensional (1D) chain (**Fig.1a**). Two kinds of five-membered rings are observed within the 1D chain, one is constructed by the pyridine nitrogen atom and its neighboring carboxylate group of $\mathbf{L}^{2-}$ ligand chelated to the Mn(II) centers, and another is constructed by the Mn(II) center and the chelating phen molecule (**Fig.1a**). Thus it is expected that the 1D chain is stable. Different chains are linked by strong π-π stacking interactions (**Table 3**) into three-dimensional (3D) supramolecular architecture (**Fig.1b**).

**(a)**

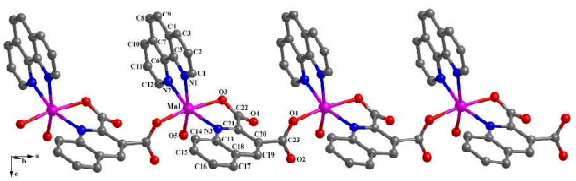

**(b)**

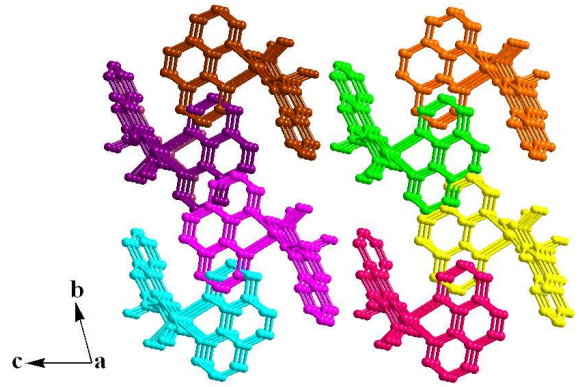


**Fig.1**. 1D chain constructed by Mn(II), $L^{2-}$ and phen in complex **1** (**a**); 3D supramolecular architecture of complex **1** constructed by strong π···π stacking interactions (**b**) (H atoms omitted for clarity).

**Crystal Structure of $Co(HL)_2(PPA)\cdot 4H_2O$ (2)** In order to investigate the relationship between the electrocatalytic activity and the structure of metal complex, by changing the species of metal(II) ions and coligands, we got another complex, $Co(HL)_2(PPA)\cdot 4H_2O$ (**2**).

**(a)**

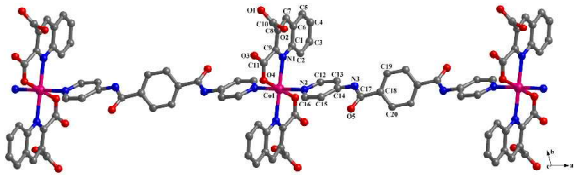

**(b)**

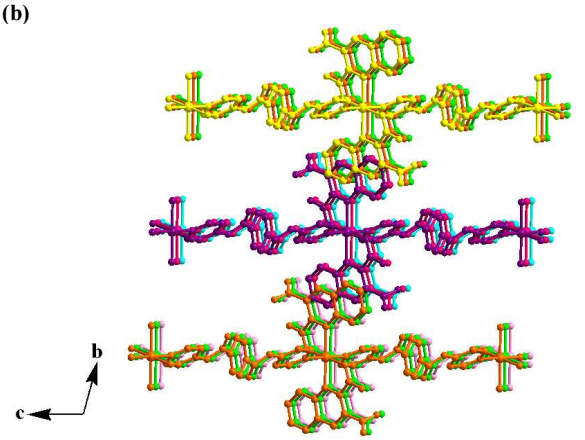


**Fig.2** 1D chain constructed by Co(II), $HL^-$ and PPA in complex **2** (**a**); 3D supramolecular architecture of complex **2** constructed by strong π···π stacking interactions (**b**) (H atoms omitted for clarity).

Complex **2** crystallizes in the *triclinic* space group *Pī* (**Table 1**), its asymmetric unit contains one independent Co(II) with 50% occupancy, one $HL^-$, half PPA and two uncoordinated water molecules. The crystallographically independent Co(1) adopts a slightly distorted octahedral coordination geometry, defined by two pyridine nitrogen atoms and two carboxylate oxygen atoms from two $HL^-$ ligands in the equatorial position, and two nitrogen atoms from two PPA ligands in the apical position [Co-O 2.0208(16) Å, Co-N 2.1594(18)- 2.2274(18) Å] (**Fig.2a** and **Table 2**). In complex **2**, $H_2L$ is partially deprotonated with its pyridine nitrogen atom and the neighboring carboxylate group chelated to the Co(II) center into a five-membered ring, leaving another carboxylate group uncoordinated (**Fig.2a**). The PPA ligand exhibits a *trans*-form linking two Co(II) centers into a 1D chain (**Fig.2a**). Strong π-π stacking interactions are observed between the above mentioned five-membered ring (Co1/O4/C11/C9/N1) and the pyridine ring (N2/C12-C16) from PPA with 4.0969(13) and 3.4773(10) Å of the centroid-centroid and perpendicular distances, respectively. Thus it is expected that the 1D chain is stable. Different chains are linked by strong hydrogen bonds and π-π stacking interactions (**Table 3**) into 3D supramolecular architecture (**Fig.2b**). For example: H2A-O2: 0.82 Å, H2A ··· O7#1: 1.765 Å, O2 ··· O7#1: 2.540 Å, ∠O2-H2A ··· O7#1: 157.1°; H17-N3: 0.86 Å, H17 ··· O3#2: 2.057 Å, N3··· O3#2: 2.902 Å, ∠N3-H17 ··· O3#2: 167.2° (Atom with additional labels #1, #2 refer to the symmetry operations: #1 x, y, z-1; #2 x-1, y, z).

The solvent-accessible volume of the unit cell of complex **2** is 86.4 $Å^3$, which is approximately 9.1 % of the unit-cell volume (945.2 $Å^3$).[14] As show in **Fig. S1**, complex **2** exhibits a 1D regular channel with a window size of ca. 3.8 × 4.5 $Å^2$.

**Electrocatalytic Activity** The XRD powder patterns of complexes **1-2** are shown in **Fig. S2** in the ESI. All the peaks of the two compounds can be indexed to their respective simulated XRD powder patterns, indicating that each of the two compounds is in pure phase. The electrodegradation of MO in the presence and absence of complexes **1** and **2** has been investigated.

In order to investigate the degradation mechanism of MO, controlled potential electrolysis (**CPE**) experiments were performed in MO aqueous solution ($7.5 \times 10^{-6}$ mol·$L^{-1}$, 50 mL) at - 1.0 V vs SCE. The solution was stirred during electrolysis experiments. At 2 h intervals, 3 mL of samples were taken out from the vessel, and subsequently analyzed by UV-visible spectroscopy. The characteristic absorption peak of MO, which is centered at 461 nm, was selected for monitoring the electrodegradation process. The characteristic absorption peak intensity of MO decreases with increasing the electrodegradation time, indicating the decrease of the MO concentration. The UV–vis absorption spectra of the MO solutions during electrolysis experiments are shown in **Fig.3.** And the changes in $C_t/C_0$ plot of the MO solutions versus reaction time were shown in **Fig.4** (wherein, $C_0$ is the initial concentration of the MO and $C_t$ is the t time's concentration of the dye).

**(a)**

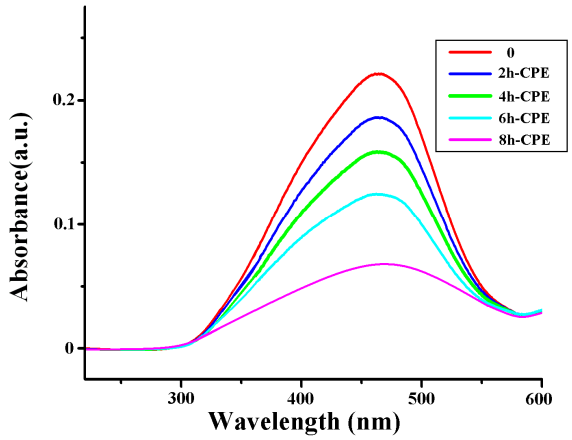


**(b)**

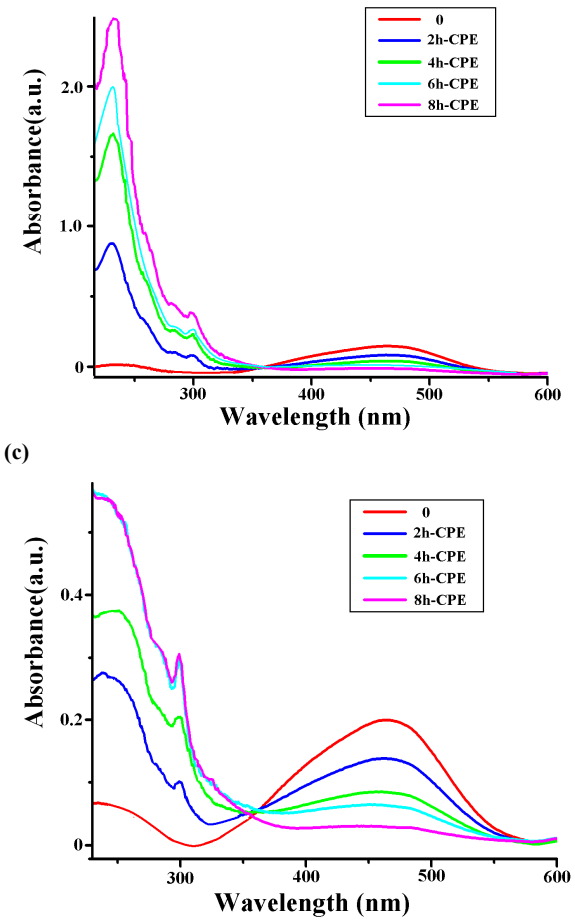


**Fig.3** The UV–vis absorption spectra of MO solutions before and after electrolysis in the absence (**a**) and presence of complexes **1** (**b**) and **2** (**c**).

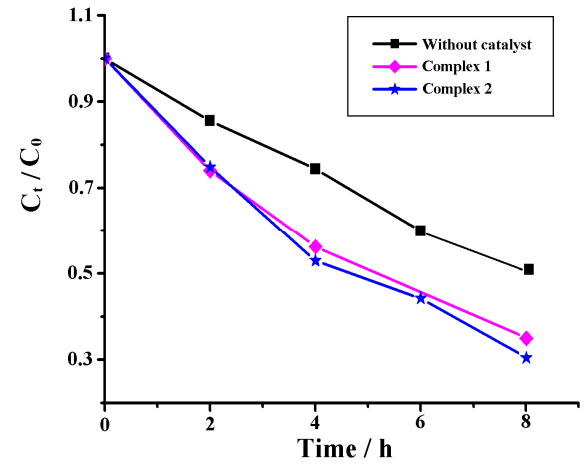


**Fig.4** Changes in $C_t/C_0$ plot of MO solutions ($7.5 \times 10^{-6}$ mol· $L^{-1}$) versus reaction time in the absence and presence of 4 mg complexes **1** and **2**.

As shown in **Figs.3a** and **4**, when the bare **GCE** was used as working electrode, it is found that MO can be decomposed to some extent without any electrocatalyst. When **1**-modified (**1-GCE**) or **2**-modified carbon glassy electrode (**2-GCE**) is used as the working electrode, the distinctly shortened degradation time indicates that complexes **1** and **2** are active for the decomposition of MO.

The optical images of the MO solutions before and after 8h-**CPE** are shown in **Fig.5**. In the presence of complexes **1** and **2**, the MO solutions show more obvious color changes than that in the blank system, indicating that complexes **1** and **2** are effective electrocatalysts for the electrodegradation of MO.

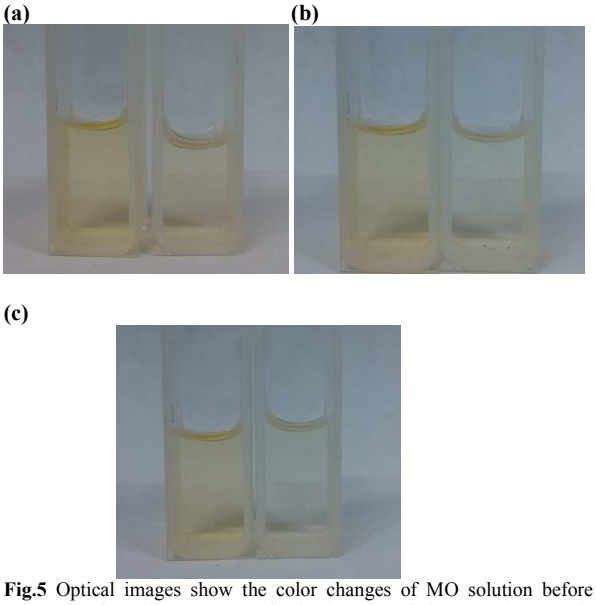


**Fig.5** Optical images show the color changes of MO solution before (**left**) and after 8h-**CPE** (**right**) in the absence of electrocatalyst (**a**), in the presence of complexes **1** (**b**) and **2** (**c**).

In order to investigate the electrocatalytic mechanisms of complexes **1** and **2**, cyclic voltammograms were performed in MO aqueous solutions before electrolysis. As shown in **Fig. 6**, it is found that both **1-GCE** and **2-GCE** show increased $H_2$ evolution reaction (HER) currents and more positive HER potentials (-1.33 V for **1-GCE** and -1.16 V for **2-GCE)** compared with the bare **GCE** (-1.38 V), indicating both complexes **1** and **2** show electrocatalytic properties for HER from water. The result is in agreement with our previous works. [11] It is probably because the charge transfer is promoted in the presence of metal complexes under HER condition. [11]

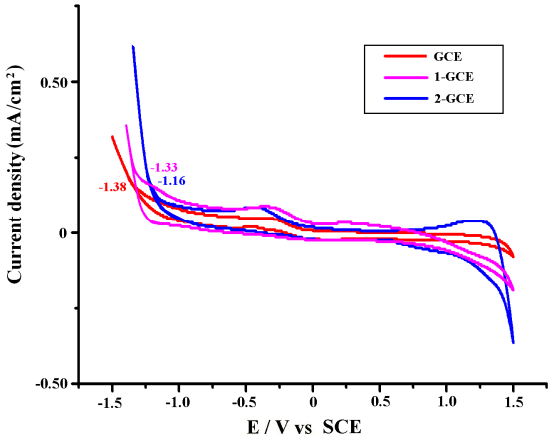


**Fig.6** Cyclic voltammograms (CVs) of the bare **GCE**, **1-GCE** and **2-GCE** in MO aqueous solution ($7.5 \times 10^{-6}$ mol·$L^{-1}$) at a sweep rate of 0.005 V·$s^{-1}$.

As we know, the mechanism of the electrodegradation of MO involves the hydroxyl radical electrocatalytically generated on the anode by the water splitting, which can be shown as follow: [4]

$2H_2O \rightarrow 2OH^* + 2H^+ + 2\,e^-$

It is expected that the improvement of the HER ($H^+ + 2e^- \rightarrow H_2$) rate in the presence of complexes **1** and **2** can promote the above reaction and thus account for the increased degradation rates of

MO. The mechanism is a bit different from that of the previously reported electrocatalysts, which catalyze the oxidation of water into OH* directly. [4-8] Herein, complexes **1** and **2** are the electrocatalysts for reduction reaction, they catalyze the reduction of $H^+$ into $H_2$ and function as indirect catalysts for the degaradation of MO.

In our case, complexes **1** and **2** were encased in Nafion and deposited on the electrode surface, as shown in **Fig. S3a** and **S3b**, respectively. After **CPE**, the solid samples left on the electrode are characterized by the powder X-ray diffraction (PXRD), which are in agreement with the simulated PXRD pattern of complexes **1** (**Fig.S2a**) and **2** (**Fig.S2b**), repectively, indicating the samples left on the electrodes retain their structural integrity**.** However, during the **CPE** experiments, both complexes **1** and **2** are partially decomposed, which can be observed in the UV-Vis spectra of the MO solutions. As shown in **Fig.3b-c**, the absorption in the UV region of 200-350 nm is attributed to the absorption of $\mathbf{L^{2-}}$ or $\mathbf{HL^-}$. The absorption peak intensity in the region increases with the increase of the electrodegradation time of MO, indicating the concentration of the ligand is increased. However, after electrocatalysis, the ligand in the solution can be reused for the syntheses of complexes **1** and **2** to obtain electrocatalysts.

**Thermal stability of complexes 1 and 2** In order to examine the thermal stability of complexes **1** and **2**, thermogravimetric analyses (TGAs) were carried out. The samples were heated up to 800 °C in Ar. As the pink curve shown in **Fig. S4**, complex **1** exhibits one step of weight loss in the range of 30-200°C with a loss of 7.6 wt% (calc. 7.4 wt%), corresponding to the loss of uncoordinated and coordinated water. The decomposition of the organic ligands began at 260 °C. As for complex **2**, it releases its uncoordinated water in the range of 30-110°C (calcd.: 8.2%; observed: 8.4%), as the blue curve shown in **Fig. S4**. The dehydrated sample remained stable up to ~230 °C without any weight loss. The decomposition of the organic components began at 230 °C, in the temperature range 230–550 °C with a loss of 83.1 wt % (calc. 83.3 wt %). The decomposition process ended at about 550 °C (**Fig.S4**).

**Gas sorption properties of complexes 1 and 2** After evacuated at 200 °C in vacuum for 8 h, gas sorption experiments of the desolvated complexes **1** and **2** were carried out.

The sorption isotherm of $N_2$ for the desolvated complex **1** at 77 K reveals a Brunauer-Emmett-Teller (BET) surface area of 6.7 $m^2 \cdot g^{-1}$, indicating it is only surface adsorption and $N_2$ molecules cannot diffuse into the channel. The result is in agreement with the crystal structure of complex **1**. As described above, complex **1** is almost nonporous and only one uncoordinated water molecule occupys the channel per unit cell of the complex.

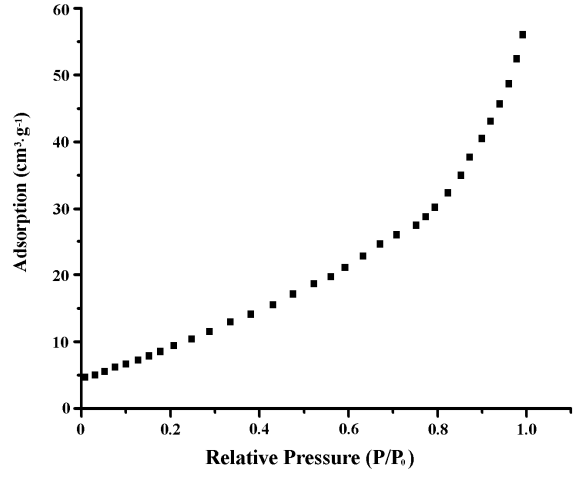


**Fig.7**. Adsorption isotherm of $N_2$ at 77 K for the dehydrated complex **2**.

As for the dehydrated complex **2**, its $N_2$ sorption isotherm at 77 K reveals a BET surface area of 56 $m^2 \cdot g^{-1}$. A plot of Horvath-Kawazoe (HK) differential pore volume indicates that complex **2** contains pore volume of ca. 0.098 $cm^3 \cdot g^{-1}$, and the desolvated complex takes up 56 $cm^3 \cdot g^{-1}$ nitrogen gas at 77 K and 1 atm (**Fig.7**). The result matchs with the catalytic activity of complex **2**. As discussed above, complex **2** shows better electrocatalytic activity for the electrodegradation of MO than complex **1**, it is probably associated with the specific surface area of complex **2**. It is expected the more specific surface area, the more exposure to MO solution, and more effective activity is obtained.

**UV-Vis absorption spectra of complexes 1 and 2** The UV-Vis absorption spectra of complexes **1-2** together with the free organic ligands in the solid state at room temperature are shown in **Fig. S5**. As shown in **Fig. S5**, $\mathbf{H_2L}$ and **PPA** exhibit strong absorption with maximum at 337 and 298 nm in the range of 240-500 nm, respectively, which probably corresponds to the n-π*or π-π* transition of the aromatic ring. [15] As for phen, it displays strong absorption peaks at 253 and 332 nm in the similar range (**Fig. S5**).

As for complex **1**, it shows absorption in the range of 240-700nm with maxima at 277 and 387 nm. As for complex **2**, it exhibits strong absorption with maxima at 313 and 535 nm in the range of 240-850nm, which are different from those of free ligands, inferring that the absorption of complexes **1** and **2** may originate from the intraligand transition (ILCT), ligand-to-ligand change transfer transition (LLCT) and metal -to- ligand charge-transfer transition (MLCT). [15]

## Conclusion

In conclusion, based on quinoline-2,3-dicarboxylic acid ($\mathbf{H_2L}$), two metal complexes formulated as $MnL(phen)(H_2O)\cdot H_2O$ (**1**) and $Co(HL)_2(PPA)\cdot 4H_2O$ (**2**) have been hydrothermally synthesized. The two metal complexes both exhibit 3D supramolecular architectures, in which 1D chains are linked by strong π-π stacking interactions. The two complexes both can increase the degradation rate of MO, it is probably associated with their electrocatalytic activities for the $H_2$ evolution reaction from water. The two complexes show different surface areas, thermal stabilities and UV-vis absorption properties.

## Supporting Information

Electronic Supplementary Information (ESI) available: PXRD patterns; TG curves; UV-vis absorption spectra in the solid state and other supplementary material.

Financial supports from the National Natural Science Foundation of China (No. 21371184) and the Fundamental Research Funds for the Central Universities (No. CQDXWL-2012-024) are gratefully acknowledged.

## References

(1) Do, J. S.; Chen, M. L. *J. Appl. Electrochem.* **1994**, *24*, 785−790.
(2) Zhan, X. M; Wang, J. L.; Wen, X. H.; Qian, Y. *Environ. Technol.* **2001**, *22*, 1105−1111.
(3) Ma, H.; Wang, B.; Luo, X. *J. Hazard. Mater.* **2007**, *149*, 492−498.
(4) (a) Panizza, M.; Cerisola, G. *Appl. Catal. B: Environ.* **2007**, *75*, 95−101; (b) Yang, Y.; Zhang, H. L.; Lee, S. M.; Kim, D.; Hwang, W.; Wang, Z. L. *Nano Lett.* **2013**, *13*, 803−808.
(5) Panizza, M.; Cerisola, G. *Environ. Sci. Technol.* **2004**, *38*, 5470−5475.
(6) Mohan, N.; Balasubramanian, N.; Basha, C. A. *J. Hazard. Mater.* **2007**, *147*, 644−651.

(7) Vecitis, C. D.; Gao, G.; Liu, H. *J. Phys. Chem. C.* **2011**, *115*, 3621−3629.
(8) Vlyssides, A. G.; Loizidous, M.; Karlis, P. K.; Zorpas, A. A.; Papaioannou, D. *J Hazard Mater,* **1999**, *B70*:41–52.
(9) (a) Leininger, S.; Olenyuk, B.; Stang, P. J. *Chem. Rev*. **2000**, *100*, 853-907; (b) Hosseini, M. W. *Acc. Chem. Res.* **2005**, *38*, 313-323; (c) Steel, P. J. *Acc. Chem. Res.* **2005**, *38*, 243-250; (d) Brammer, L. *Chem. Soc. Rev.* **2004**, *33*, 476-489; (e) Seidel, S. R.; Stang, P. J. *Acc. Chem. Res*. **2002**, *35*, 972-983; (f) Janiak, C. *Coord. Chem. Rev.* **2006**, *250*, 66-94; (g) Blank, F.; Janiak, C. *Coord. Chem. Rev*. **2009**, *253*, 827-1220.
(10) (a) Caulder, D. L.; Raymond, K. N. *Acc. Chem. Res*. **1999**, *32*, 975-982; (b) Khlobystov, A. N.; Blake, A. J.; Champness, N. R.; Lemenovskii, D. A.; Majouga, A. G.; Zyk, N. V.; Schröder, M. *Coord. Chem. Rev.* **2001**, *222*, 155-192; (c) Moulton, B.; Zaworotko, M. J. *Chem. Rev*. **2001**, *101*, 1629-1658; (d) Yaghi, O. M.; O'Keeffe, M.; Ockwig, N. W.; Chae, H. K.; Eddaoudi, M.; Kim, J. *Nature* **2003**, *423*, 705-714; (e) Zheng, S. T.; Zhang, J.; Li, X. X.; Fang, W. H.; Yang, G. Y. *J. Am. Chem. Soc.* **2010**, *132*, 15102-15103.
(11) (a) Gong, Y.; Wu, T.; Jiang, P. G.; Lin, J. H.; Yang, Y. X. *Inorg. Chem.* **2013**, *52*, 777-784; (b) Gong, Y.; Shi, H. F.; Hao, Z.; Sun, J. L.; Lin, J. H. *Dalton Trans.* **2013**, *42*, 12252-12259; (c) Gong, Y.; Hao, Z.; Shi, H. F.; Jiang, P. G.; Zhang, M. M.; Lin, J. H. *ChemPlusChem* DOI: 10.1002/cplu.201300334.
(12) Moriconi, E. J.; Spano, F. A. *J. Am. Chem. Soc*. **1964**, *86*, 38-46.
(13) (a) Sheldrick, G. M. *SHELXS 97, Program for Crystal Structure Solution*, University of Göttingen, Göttingen, Germany, **1997**; (b) Sheldrick, G. M. *SHELXL 97, Program for Crystal Structure Refinement*, University of Göttingen, Göttingen, Germany, **1997**.
(14) Friedrichs, O. D.; O'Keeffe, M.; Yaghi, O. M. *Acta Crystallogr. A* **2003**, *59*, 22−27.
(15) (a) Ohkoshi, S.; Tokoro, H.; Hozumi, T.; Zhang, Y.; Hashimoto, K.; Mathonière, C.; Bord, I.; Rombaut, G.; Verelst, M.; Moulin, C. C.; Villain, F. *J. Am. Chem. Soc*. **2006**, *128*, 270-277; (b) Censo, D. D.; Fantacci, S.; Angelis, F. D.; Klein, C.; Evans, N.; Kalyanasundaram, K.; Bolink, H. J.; Grätzel, M.; Nazeeruddin, M. K. *Inorg. Chem*. **2008**, *47*, 980-989; (c) Wang, J. H.; Fang, Y. Q.; Bourget-Merle, L.; Polson, M. I. J.; Hanan, G. S.; Juris, A.; Loiseau, F.; Campagna, S. *Chem. Eur. J*. **2006**, *12*, 8539-8548.

**Table 3** The centroid-centroid (CC) distance (Å) and perpendicular (P) distance (Å) involving π···π stacking interactions for complexes **1-2**.

| *Plane* | *Plane* | *CC distance* | *P distance* |
|---|---|---|---|
| | *Complex **1*** | | |
| N1/C1-C5 | N1A/C1A-C5A | 3.644(3) | 3.502(19) |
| N2/C6-C7/C10-C12 | N2B/C6B-C7B/C10B-C12B | 3.681(3) | 3.503(2) |
| N2/C6-C7/C10-C12 | C4B-C9B | 3.850(3) | 3.557(2) |
| N3/C13/C18-C21 | C13D-C18D | 3.787(3) | 3.588(2) |
| | *Complex **2*** | | |
| Co1/O4/C9/C11/N1 | N2E/C12E-C16E | 4.097(13) | 3.477(10) |
| N1/C1/C6-C9 | N1D/C1D/C6D-C9D | 4.044(15) | 3.841(10) |
| C1-C6 | C1F-C6F | 3.826(15) | 3.481(11) |

Symmetry transformations used to generate equivalent atoms:
A 2-x, 1-y, 2-z B 1-x, 2-y, 2-z D 1-x, 1-y, 1-z E 1-x, 2-y, 1-z F -x, 1-y, 1-z